


NUCLEAR MEDICINE



# Glucose metabolic rate from four-dimensional [ $^{18}\text{F}$ ]FDG PET/CT to differentiate sarcoid lesions from malignant lesions

Akihiro Inoue<sup>1</sup>, Michinobu Nagao<sup>1\*</sup> , Koichiro Kaneko<sup>1</sup>, Atsushi Yamamoto<sup>1</sup>, Yurie Shirai<sup>1</sup>, Ohno Toshihiro<sup>1</sup>, Akiko Sakai<sup>2</sup>, Risa Imakado<sup>2</sup> and Shuji Sakai<sup>1</sup>

## Abstract

**Objectives** On  $^{18}\text{F}$ -Fludeoxyglucose (FDG) PET/CT, active sarcoid lesions are often difficult to differentiate from malignant lesions. We investigated the potential of the glucose metabolic rate ( $\text{MR}_{\text{glc}}$ , mg/min/100 mL), a new quantification of glucose metabolic kinetics derived from direct reconstruction based on linear Patlak analysis, to distinguish between sarcoidosis and malignant lesions.

**Materials and methods** A total of 100 patients with cardiac sarcoidosis (CS) and 67 patients with cancer who underwent four-dimensional FDG PET/CT were enrolled. The lesions with a standardized uptake value (SUV)  $\geq 2.7$  on the standard scan were included as active lesions in the analysis. SUV and  $\text{MR}_{\text{glc}}$  were derived using data acquired between 30 min and 50 min on four-dimensional FDG PET/CT. The mean value in the volume of interest (size 1.5 cm<sup>3</sup>) was measured. The diagnostic performance of sarcoidosis using  $\text{MR}_{\text{glc}}$  and SUV was evaluated using receiver-operating-characteristic (ROC) analysis.

**Results** A total of 90 sarcoidosis lesions from 44 CS patients (18 males,  $63.4 \pm 12.2$  years) and 87 malignant lesions from 57 cancer-bearing patients (32 males,  $65 \pm 14$  years) were analyzed. SUV and  $\text{MR}_{\text{glc}}$  for sarcoid lesions were significantly lower than those for malignant lesions (SUV,  $4.98 \pm 2.00$  vs  $6.21 \pm 2.14$ ;  $\text{MR}_{\text{glc}}$ ,  $2.52 \pm 1.39$  vs  $3.68 \pm 1.61$ ;  $p < 0.01$ ). ROC analysis indicated that the ability to discriminate sarcoid patients from those with malignancy yielded areas under the curves of 0.703 and 0.754, with sensitivities of 64% and 77% and specificities of 75% and 72% for SUV 5.025 and  $\text{MR}_{\text{glc}}$  2.855, respectively.

**Conclusion**  $\text{MR}_{\text{glc}}$  was significantly lower in sarcoid lesions than malignant lesions, and improved sarcoid lesions identification over SUV alone.

**Clinical relevance statement**  $\text{MR}_{\text{glc}}$  improves sarcoid lymph node identification over SUV alone and is expected to shorten the examination time by eliminating delayed scans.

## Key Points

- Active sarcoid lesions are sometimes associated with FDG accumulation and should be differentiated from malignant lesions.
- SUV and metabolic rate of glucose ( $\text{MR}_{\text{glc}}$ ) strongly positively correlated, and  $\text{MR}_{\text{glc}}$  could differentiate sarcoid and malignant lesions.
- $\text{MR}_{\text{glc}}$  allows for accurate evaluation and staging of malignant lesions.

**Keywords** FDG-PET, Sarcoidosis, Malignant tumor,  $\text{MR}_{\text{glc}}$ , Patlak reconstruction

\*Correspondence:

Michinobu Nagao

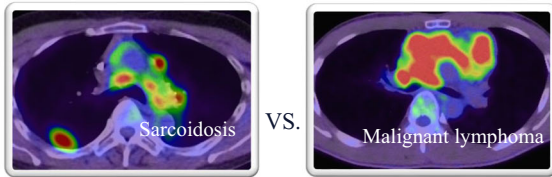
[nagao.michinobu@twmu.ac.jp](mailto:nagao.michinobu@twmu.ac.jp)

<sup>1</sup>Department of Diagnostic Imaging and Nuclear Medicine, Tokyo Women's Medical University, Tokyo, Japan

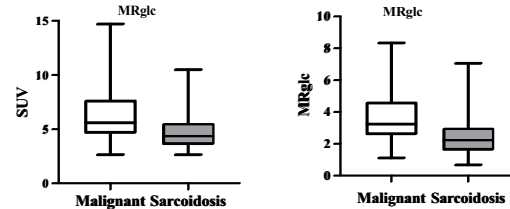
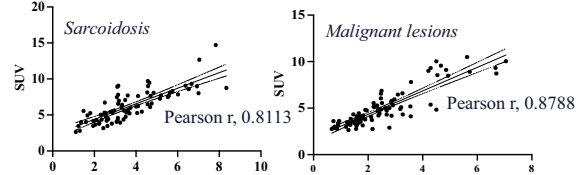
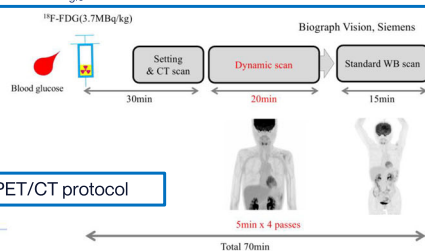
<sup>2</sup>Department of Cardiology, Tokyo Women's Medical University, Tokyo, Japan

## Graphical Abstract

### Glucose metabolic rate from four-dimensional $[^{18}\text{F}]\text{FDG}$ PET/CT to differentiate sarcoid lesions from malignant lesions



The accumulation of active sarcoid lymph nodes is often difficult to differentiate from malignant lesions in FDG PET/CT. The purpose of this study is to differentiate active sarcoid lymph nodes from malignant lesions, and we investigate the diagnostic ability of  $\text{MR}_{\text{glc}}$  compared to conventional SUV.



SUV and  $\text{MR}_{\text{glc}}$  for sarcoid lymph nodes were significantly lower than those for malignant lesions. The ability to discriminate sarcoid patients from malignant patients were AUC of 0.703 and 0.754, 64% and 77% sensitivities, and 75% and 72% specificities for SUV 5.025 and  $\text{MR}_{\text{glc}}$  2.855, respectively.

European  
Radiology

Eur Radiol (2024) Inoue A, Nagao M, Kaneko K et al.  
DOI: 10.1007/s00330-024-11022-w

### Introduction

$[^{18}\text{F}]$  Fluorodeoxyglucose (FDG) PET/CT has contributed to the diagnosis of active inflammation in patients with cardiac sarcoidosis (CS) [1]. Active granulomatous conditions with the aggregation of inflammatory cells in sarcoidosis result in FDG accumulation, and it has been suggested that the intensity of FDG uptake may reflect disease activity [2–5]. Malignant diseases such as lymphoma, and lymphatic metastasis are common causes of lymphadenopathy and intense FDG accumulation. In the diagnostic modality of FDG PET/CT, the accumulation of active sarcoid lymph nodes is often difficult to differentiate from malignant diseases [5, 6].

When we assessed active inflammation in the CS, visual and semi-quantitative assessments were generally performed using static imaging after a certain uptake period by measuring the standardized uptake value (SUV) [1, 3]. Recently, the introduction of new-generation PET/CT scanners, such as silicon photomultiplier (SiPM)-based PET/CT scanners and sophisticated software for data analysis, has facilitated the widespread application of four-dimensional FDG PET/CT imaging in clinical oncology. Using a four-dimensional analysis, a SiPM FDG PET scan can provide information regarding metabolic parameters [7]. Four-dimensional FDG PET/CT is a

recently developed technique that provides the four-dimensional PET data required for the direct reconstruction of multiparametric images based on linear Patlak analysis. Multiparametric imaging enhances the standard SUV by introducing two new parametric images: glucose metabolic rate ( $\text{MR}_{\text{glc}}$ , mg/min/100 mL) and distribution volume (DV, %) of free FDG in the tissue [8–11].  $\text{MR}_{\text{glc}}$  is a new quantification index of glucose metabolic kinetics derived from a four-dimensional SiPM FDG PET scan and is related to the transport/phosphorylation-dependent part of FDG [9–11]. The free FDG available before the start of FDG phosphorylation is reflected by DV, which estimates the vascularity and interstitial fluid components of the tissue being evaluated [9–11]. Recent studies have demonstrated that oncologic  $\text{MR}_{\text{glc}}$  images offer superior lesion contrast or detectability and reduce false-positive rates compared with SUV imaging [9, 12].

Although there are some reports on the differentiation between sarcoidosis and malignant lesions using SUV [6, 9, 12–14], the utility of  $\text{MR}_{\text{glc}}$  has yet to be investigated. We hypothesized that parametric analyses using four-dimensional FDG PET/CT imaging could differentiate sarcoids from malignant lesions precisely. In this study, we compared and verified the ability of  $\text{MR}_{\text{glc}}$  and

**Table 1** Overview of patient characteristics

	Sarcoidosis	Malignant lesions
Patients ( <i>n</i> )	44	57
Sex (M/F)	18/26	32/25
Mean age (y) [range]	63.4 ± 12.2 [35–87]	65 ± 14 [26–86]
Number of lesions	90	87
Measurement site		
Hilar/mediastinal lymph nodes	73	11
Lung	1	6
Abdominal lymph node	11	6
Liver	1	45
Others (primary lesion)	4	19 (12)
Measurement of FDG		
Average of SUV [range]	4.7 ± 1.9 [2.7–9.7]	6.0 ± 1.9 [2.8–11.2]
Average of MR <sub>glc</sub> [range]	2.4 ± 1.3 [0.67–6.2]	3.6 ± 1.4 [1.3–6.7]

Basic patient characteristics and FDG-PET measurement data of FDG in sarcoidosis and malignant lesions are provided  
 FDG [<sup>18</sup>F] fluorodeoxyglucose, MR<sub>glc</sub> glucose metabolic rate, SUV standardized uptake value

conventional SUV to distinguish between sarcoidosis and malignant lesions.

## Materials and methods

This single-center, retrospective, cross-sectional study evaluated the MR<sub>glc</sub>'s diagnostic ability in differentiating active sarcoid lymph nodes from malignant lesions. It was conducted in accordance with the declaration of Helsinki (revised in 2013). The study protocol was approved by our hospital's ethics committee. Written informed consent was obtained from all the patients.

### Study population

In this study, 100 patients with CS (49 males and 51 females, mean age 62.3 ± 13.7 years) and 68 patients with cancer (42 males and 26 females, mean age 65.6 ± 14.3 years) who underwent four-dimensional FDG PET/CT scan between March 2021 and September 2023 in our hospital were enrolled. For patients with cancer, PET/CT scans at initial diagnosis or pre-treatment PET/CT scans at the time of relapse in patients with a complete response (CR) were included in the analysis. Patients with CS were diagnosed according to the guidelines of the Japanese Circulation Society for diagnosing and treating CS [15]. For CS, images obtained at the initial diagnosis before steroid treatment were included in the analysis. The clinical characteristics of the patients are summarized in Table 1. No pathological examination has been performed to differentiate between sarcoid-like reactions in sarcoidosis. The patients with cancer included nine with colon cancer, nine with rectal cancer, six with breast

**Table 2** Breakdown of primary tumors in malignant patients

Primary site, ( <i>n</i> = 57)	Number
Colon cancer	9
Colon cancer and gastric cancer	2
Rectal cancer	9
Breast cancer	6
Gastric cancer	5
Hepatocellular carcinoma	4
Pancreas cancer	4
Lung cancer	3
Cholangiocarcinoma	3
Lymphoma, renal cancer, thymic cancer, and uterine cancer	2
Esophageal cancer, gastric GIST, ovarian cancer, and ureter cancer	1

GIST gastrointestinal stromal tumor

cancer, five with gastric cancer, and others. Patients have various types of cancer. The study population included two patients with coexisting colon and gastric cancers (Table 2). Patients with 150 mg/dL of serum glucose levels and incomplete four-dimensional PET/CT data were excluded from the study.

### Four-dimensional [<sup>18</sup>F]FDG PET/CT scan with a semiconductor scanner

All FDG PET/CT scans were performed using a Biograph Vision 600 PET/CT scanner (Siemens Healthineers), which integrates a 64-slice multi-detector CT using a fully automated multiparametric PET acquisition protocol (Flow Motion Multiparametric PET, Siemens Healthineers). The preparation included 18 h of fasting for patients with CS and 6 h for those with cancer and receiving an intravenous injection of FDG (3.7 MBq/kg). All patients in the CS group were fed a high-fat, low-carbohydrate diet before FDG PET/CT based on the recommendations of the Japanese Society of Nuclear Cardiology [15].

A whole-body imaging protocol was used to acquire PET data. First, a low-dose non-contrast-enhanced CT was performed for attenuation correction, covering the top of the skull to the proximal thigh. Shortened multiparametric PET acquisition, which consisted of 4 × 5 min (total 20 min, 30–50 min post-FDG injection) of continuous bed motion passes, was performed according to previous studies [16, 17]. After 60 min, a standard scan was performed. Four-dimensional PET data acquisition is a prerequisite for calculating parametric images that reflect specific pharmacokinetic parameters [18]. The multiparametric scan protocol generates parametric images based on the Patlak model [19], with the parameters being the Patlak slope ( $K_i$ ), which represents the

rate of irreversible uptake, and the Patlak intercept (DV), which indicates the apparent DV of non-metabolized tracers. Parametric images of the metabolic rate of FDG (MR<sub>glc</sub>) and DV were generated using list-mode data from the last four passes (30–50 min) scanned by the PET/CT scanner and the population-based input function method from the five passes (0–30 min) provided by the PET/CT scanner [16, 17, 20, 21]. The static scans reconstructed the emission data using a time-of-flight point-spread-function algorithm with four iterations and five subsets. The Patlak slope based on the linear Patlak analysis, which represents the constant influx rate of FDG (Ki), was multiplied by the blood glucose level and divided by the lumped constant (LC) to calculate the MR<sub>glc</sub>. The LC was fixed at 1.0 in our hospital. A Gaussian filter was applied, and the in-plane spatial resolutions (full width at half maximum) was 4 mm.

#### Measuring SUV and MR<sub>glc</sub>

Parametric Patlak and SUV images were semi-quantitatively analyzed by experienced nuclear physicians (M.N. with 33 years of experience and K.K. with 26 years of experience) using Syngo via software version VB30A\_HF08 (Siemens Healthineers). Using a parametric horizontal-axial image, the mean values within the volume of interest (size 1.5 cm<sup>3</sup>) of the MR<sub>glc</sub> and SUV were measured for active lesions. In patients with sarcoidosis and cancer, lesions with SUV<sub>mean</sub> ≥ 2.7 were considered active and included in the analysis [22]. Lesions were selected in descending order of SUV value, with a limit of three per patient. At least one lymph node was measured in the sarcoidosis group, including the right and left pulmonary hila and mediastinum. If there was no accumulation in the thoracic lymph nodes, abdominal lymph nodes, or nodular accumulation in the liver or spleen were selected. In the malignant group, mediastinal hilar lymph node and lung metastases were selected first, followed by abdominal lymph node, liver metastasis, and primary liver lesions.

#### Statistical analysis and evaluation items

Continuous data are expressed as a mean ± standard deviation. The following items were evaluated:

1. A comparison of PET measurements between sarcoidosis and the malignant group was performed using the Mann–Whitney *U*-test.
2. Pearson's coefficient analysis was used to determine the correlation between SUV and MR<sub>glc</sub>.
3. Receiver operating characteristic (ROC) curve analysis was performed to determine the optimal cutoff values of SUV and MR<sub>glc</sub> for detecting sarcoidosis and to investigate the area under the curve (AUC), sensitivity, and specificity.

All statistical tests conducted were two-sided. Statistical significance was set at  $p < 0.05$ . All statistical analyses were performed using JMP version 16.0 (SAS Institute).

## Results

### Correlation between SUV and MR<sub>glc</sub>

The analysis included 90 sarcoidosis lesions from 44 of 100 patients with CS (18 males and 26 females, mean age, 63.4 ± 12.2 years) and 87 malignant lesions from 57 of 67 patients with cancer (32 males and 25 females, mean age, 65 ± 14 years) were included in the analysis (Fig. 1). In the sarcoidosis group, the average number of lesions per patient was 2.0 and in the malignant group, 1.5. In both the sarcoidosis and malignant groups, MR<sub>glc</sub> was strongly positively correlated with SUV (sarcoidosis and malignancy: Pearson's  $r$ , 0.8788 and 0.8113,  $p < 0.01$ ) (Fig. 2).

### Diagnostic performance of sarcoidosis using SUV and MR<sub>glc</sub>

Moreover, SUV and MR<sub>glc</sub> for sarcoid lesions were significantly lower than those for malignant lesions (SUV, 4.98 ± 2.00 vs 6.21 ± 2.14; MR<sub>glc</sub>, 2.52 ± 1.39 vs 3.68 ± 1.61;  $p < 0.01$ ). ROC analysis revealed that the ability to discriminate sarcoid lesions from malignant lesions yielded an AUC of 0.694, with 54% sensitivity, and 75% specificity for SUV of 4.715, and an AUC of 0.735, with 61% sensitivity, and 81% specificity for MR<sub>glc</sub> of 2.475 (Fig. 3).

Lesions with the highest SUV among multiple lesions per patient were considered representative. Furthermore, SUV and MR<sub>glc</sub> for patients with sarcoid lesions were significantly lower than those for patients with malignant lesions (SUV, 5.07 ± 2.14 vs 6.47 ± 2.31; MR<sub>glc</sub>, 2.55 ± 1.52 vs 3.84 ± 1.70;  $p < 0.01$ ). The optimal cutoff values of SUV and MR<sub>glc</sub> were 5.025 and 2.855, respectively. The values that distinguished patients with sarcoid lesions from those with malignant lesions had AUC of 0.703 and 0.754, sensitivities of 64% and 77%, and specificities of 75% and 72%, respectively (Fig. 4). The average number of multiple lesions per patient was used as the representative value. SUV and MR<sub>glc</sub> for patients with sarcoid lesions were significantly lower than those for patients with malignant lesions (SUV, 4.77 ± 1.91 vs 6.04 ± 1.92; MR<sub>glc</sub>, 2.42 ± 1.36 vs 3.55 ± 1.42;  $p < 0.01$  for all). The optimal cut-off values of SUV and MR<sub>glc</sub> were 4.858 and 2.475, respectively. The values distinguishing patients with sarcoid lesions from those with malignant lesions had AUC of 0.717 and 0.746, sensitivities of 66% and 66%, and specificities of 72% and 79%, respectively. Two representative cases of sarcoidosis and malignant lesions are shown in Figs. 5 and 6, respectively.

## Discussion

This is the first study to differentiate active sarcoid lesions from malignant lesions using parametric analysis

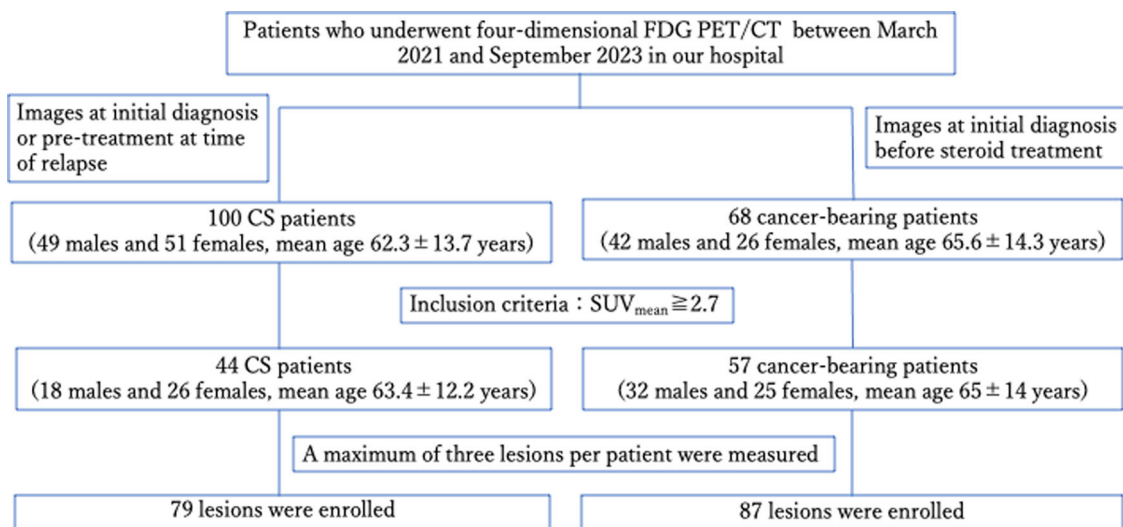


**Fig. 1** Patient entry flowchart. One hundred patients with CS and 68 cancer-bearing patients who underwent four-dimensional FDG PET/CT between March 2021 and September 2023 at our hospital were enrolled in this study. Lesions with  $SUV_{mean} \geq 2.7$  were considered active and included in the analysis and a maximum of three lesions per patient were measured. CS, cardiac sarcoidosis; SUV, standardized uptake value; FDG, [ $^{18}F$ ] fluorodeoxyglucose

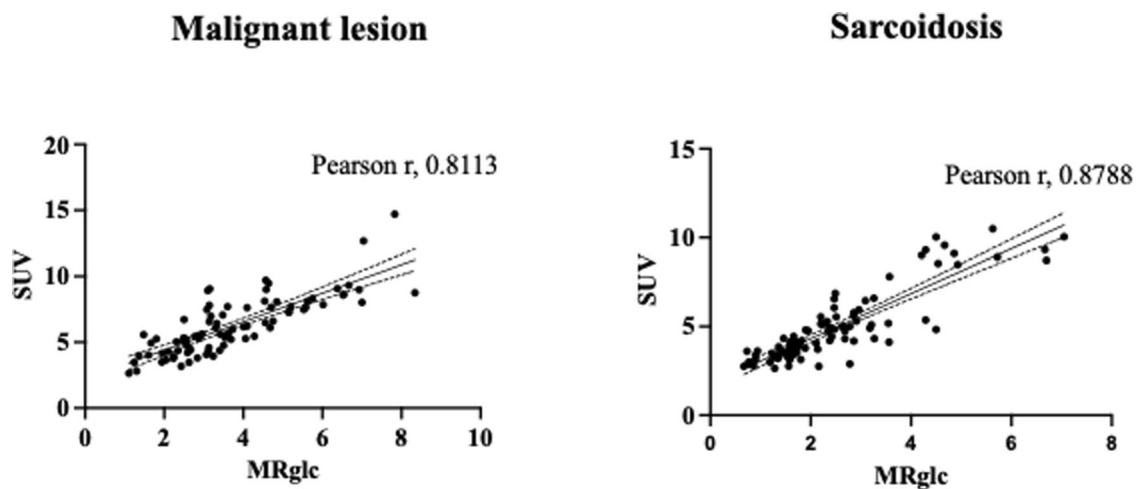


**Fig. 2** (Left) Correlation between SUV and  $MR_{glc}$  in malignant lesions.  $MR_{glc}$  was strongly positively correlated with SUV (Pearson  $r$ , 0.8113,  $p < 0.01$ ). (Right) Correlation between SUV and  $MR_{glc}$  in sarcoid lesions.  $MR_{glc}$  was strongly positively correlated with SUV (Pearson  $r$ , 0.8788,  $p < 0.01$ ).  $MR_{glc}$ , glucose metabolic rate; SUV, standardized uptake value

of four-dimensional FDG PET/CT imaging and to investigate the diagnostic performance of  $MR_{glc}$ . Our results demonstrated that (1)  $MR_{glc}$  was strongly positively correlated with SUV in sarcoidosis and malignant lesions, (2) sarcoidosis lesions demonstrated lower SUV and  $MR_{glc}$  values than malignant lesions, and (3)  $MR_{glc}$  displayed higher AUCs for differentiating sarcoid lymph nodes from malignant lesions than SUV images, suggesting its utility in differentiating sarcoid lesions from malignant lesions. These results will improve the accuracy of metastatic

lymph node diagnosis in cancer patients and contribute to detecting malignant tumors that complicate sarcoidosis. As shown in Fig. 5b, c, the contrast of the lesion in the  $MR_{glc}$  image without large vessel accumulation was much clearer than in the SUV image. Differentiation from physiological myocardial accumulation is often problematic for detecting active lesions in CS. In this study's patients with CS, the contrast ratio of active myocardial lesions to normal myocardium averaged 5.8 on  $MR_{glc}$  images, compared to an average of 2.4 on SUV images.

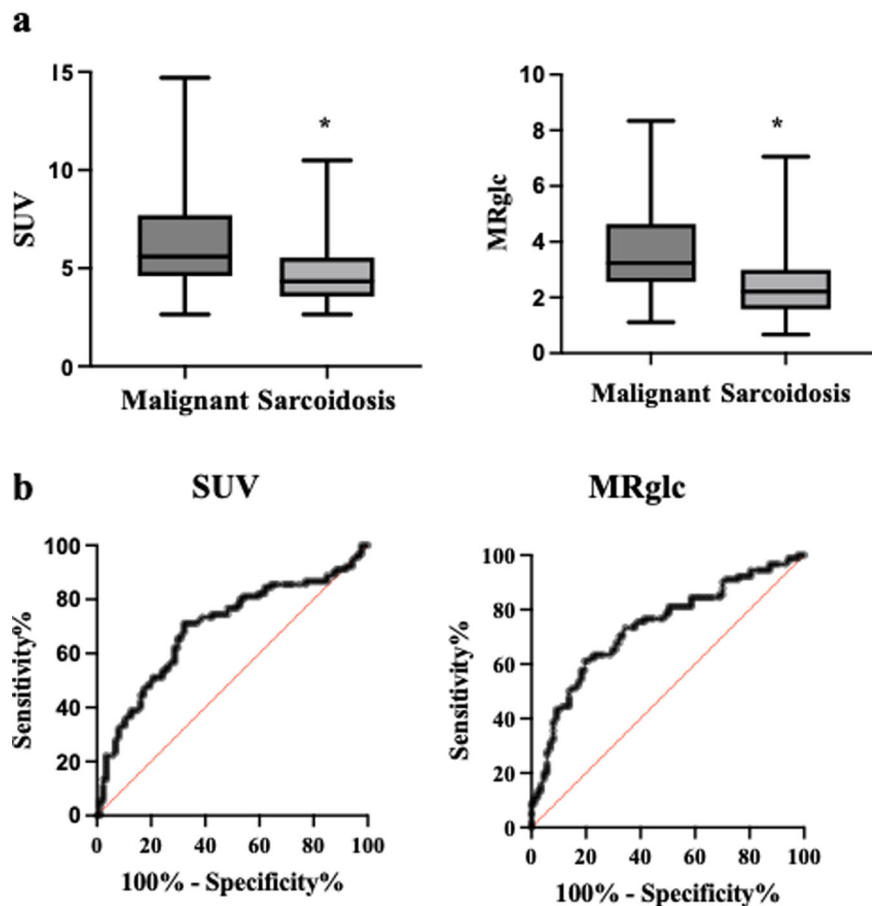


**Fig. 3 a** (Left) Box-and-whisker plots of SUV for sarcoidosis lesions and malignant lesions. SUV for sarcoid lesions was significantly lower than those for malignant lesions ( $4.98 \pm 2.00$  vs  $6.21 \pm 2.14$ ;  $*p < 0.01$ ). (Right) Box-and-whisker plots of  $MR_{glc}$  for sarcoidosis lesions and malignant lesions.  $MR_{glc}$  for sarcoid lesions were significantly lower than those for malignant lesions ( $2.52 \pm 1.39$  vs  $3.68 \pm 1.61$ ;  $*p < 0.01$ ). **b** (Left) The diagnostic performance of sarcoidosis lesions using SUV. ROC analysis revealed that the ability to discriminate sarcoid and malignant lesions yielded an AUC of 0.694, with 54% sensitivity and 75% specificity for SUV 4.715. (Right) The diagnostic performance of sarcoidosis lesions using  $MR_{glc}$ . ROC analysis revealed that the ability to discriminate sarcoid and malignant lesions yielded an AUC of 0.735, with 61% sensitivity and 81% specificity for  $MR_{glc}$  2.475. AUC, the area under the curve;  $MR_{glc}$ , glucose metabolic rate; ROC, receiver operating characteristic; SUV, standardized uptake value

$MR_{glc}$  imaging has the advantage of suppressing physiological myocardial accumulation and better localizing active myocardial lesions. This FDG-PET protocol affects the patient throughput because it extends the overall scan time from 30 min after FDG administration to the end of the standard whole-body scan. However, by consolidating the evidence of the usefulness of parametric analysis, such as  $MR_{glc}$  images with a semiconductor PET system, it will be possible to shorten or eliminate the standard scan at 1 h after FDG administration in the future.

Four-dimensional FDG PET/CT produces two parametric images:  $MR_{glc}$  images, which represent the metabolic rate of FDG in the tissue, and DV images which represent the DV of free FDG in the reversible compartments and the fractional blood volume. These images differentiate free FDG and bound FDG-6-phosphate (FDG-6-P) [9]. Previous four-dimensional FDG PET/CT

studies have demonstrated that  $MR_{glc}$  images have good visual quality, superior lesion contrast, and reduced false-positive rates when complementing standard SUV imaging [9, 12]. However, the quantitative superiority of lesion detection by  $MR_{glc}$  imaging does not translate to the detection of more lesions; that is, the sensitivity of  $MR_{glc}$  imaging is equal to that of SUV imaging. Parametric imaging of free tracers using DV images allows the correct identification of small SUV image foci as artifacts, thereby increasing the specificity of FDG PET/CT [9]. Recent studies have demonstrated an excellent correlation between the values in malignant and benign lesions between  $MR_{glc}$  and SUV images [9, 12]. Our results also confirmed that  $MR_{glc}$  positively correlated with SUV in sarcoidosis and malignant lesions.

The two significant proteins unequivocally associated with increased FDG uptake in cancers are glucose

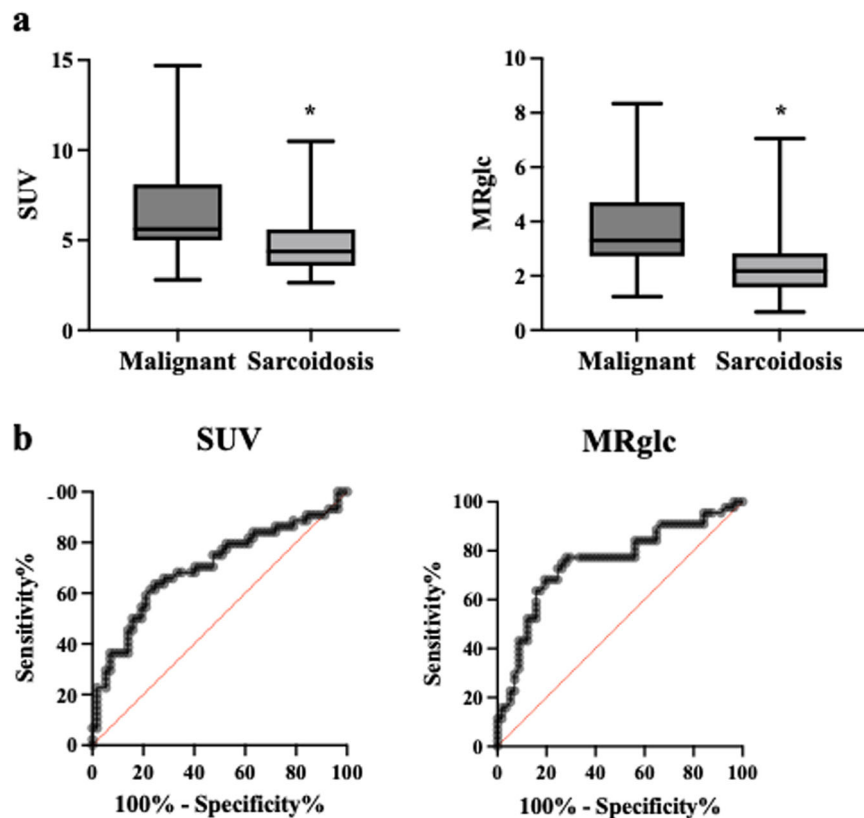


**Fig. 4 a** (Left) Box-and-whisker plots of SUV for patients with sarcoidosis lesions and malignant lesions. SUV for patients with sarcoid lesions was significantly lower than that for malignant lesions ( $5.07 \pm 2.14$  vs  $6.47 \pm 2.31$ ;  $*p < 0.01$ ). (Right) Box-and-whisker plots of  $MR_{glc}$  for patients with sarcoidosis lesions and malignant lesions.  $MR_{glc}$  for patients with sarcoid lesions was significantly lower than that for malignant lesions ( $2.55 \pm 1.52$  vs  $3.84 \pm 1.70$ ;  $*p < 0.01$ ). **b** (Left) The diagnostic performance of patients with sarcoidosis lesions using SUV. ROC analysis revealed that the ability to discriminate patients with sarcoid and malignant lesions yielded an AUC of 0.703, with 64% sensitivity and 75% specificity for SUV 5.025. (Right) The diagnostic performance of patients with sarcoidosis lesions using  $MR_{glc}$ . ROC analysis revealed that the ability to discriminate sarcoid and malignant lesions yielded an AUC of 0.754, with 77% sensitivity and 72% specificity for  $MR_{glc}$  2.855. AUC, the area under the curve;  $MR_{glc}$ , glucose metabolic rate; ROC, receiver operating characteristic; SUV, standardized uptake value

transporter (GLUT-1) and hexokinase (HK, primarily HK-2) [23]. FDG is incorporated into cancer cells via GLUT-1 activity, and HK-2 causes subsequent intracellular accumulation of FDG. Similarly, in stimulated inflammatory cells, such as in sarcoidosis, in addition to increased expression of GLUT, HK, which mediates the phosphorylation of intracellular FDG and results in its retention within cells, is translocated to the endofacial surface of GLUT and is activated [1, 23, 24]. HK-2 efficiently phosphorylates glucose to glucose-6-P using energy produced by the mitochondria. Similarly, FDG is phosphorylated from FDG-6-P. HK activity is higher in malignant tumors than during inflammation [25]. Glycolytic enzymes, such as HK and phosphofruktokinase, have been reported to be upregulated in many cancer types [23, 26]. The HK-2 isoform is notable because it reversibly binds to mitochondria and serves as a critical regulator of glycolysis and survival in multiple cancers,

where it is a poor prognostic indicator [23]. Furthermore, the low activity of glucose-6-phosphatase, which hydrolyzes FDG-6-P to FDG in tumor cells, leads to the tumor cell accumulation of FDG-6-P [21, 24]. Thus, the characteristics of the activity of glucose metabolic enzymes in sarcoidosis and malignant lesions are believed to be the reasons for the lower  $MR_{glc}$  in sarcoidosis.

This study has some limitations. First, the fasting time for patients with sarcoidosis was 18 h, whereas that for patients with cancer was 6 h, indicating a difference in the preparation protocol. Because differences in fasting time are a crucial factor in glucose metabolism, we measured the SUV values in the descending thoracic aorta and standard uptake ratio (SUR) values in the lesions to clarify this issue. SUR is helpful for the reproducibility of quantitative data and is also known as the tumor-to-background ratio using image-derived internal standards. The SUR correlates more with the metabolic rate of glucose than with the SUV [27].

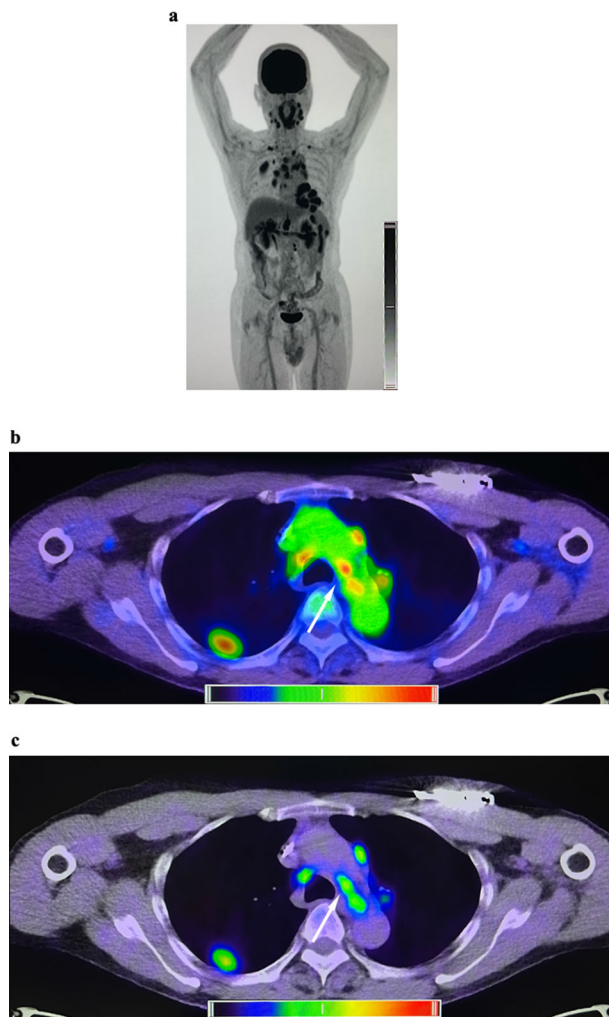


**Fig. 5** A case of a 50-year-old female with active CS and lymph node lesions. MIP image (**a**) demonstrated accumulations in bilateral hilar lymph nodes and mediastinal lymph nodes, and multiple focal accumulations in the heart. FDG (**b**) and MR<sub>glc</sub> (**c**) images show low FDG uptake in mediastinal lymph nodes (SUV = 3.65, MR<sub>glc</sub> = 1.58). Focal FDG uptake is seen in each image's right upper lobe (pulmonary sarcoidosis). The gray and color calibration scales are shown in the figure. For each scale's window bottom and top values, SUV values were bottom = 0, and top = 5 [SUV-bw], and MR<sub>glc</sub> was bottom = 0 and top = 4 [mg/min/100 mL]. CS, cardiac sarcoidosis; FDG, [<sup>18</sup>F] fluorodeoxyglucose; MIP, maximum intensity projection; MR<sub>glc</sub>, glucose metabolic rate; SUV, standardized uptake value

We randomly selected 20 patients from the malignancy and sarcoidosis groups based on the SUV of the descending thoracic aorta and calculated the SUR of the lesion with the highest SUV. As a result, the SUR of the malignancy group was  $2.77 \pm 1.04$ , and that of the sarcoidosis group was  $2.52 \pm 0.98$  ( $p = 0.318$ ), showing no significant difference. On the other hand, the SUV values for the descending aorta were almost identical,  $2.30 \pm 0.22$  for the malignancy group and  $2.27 \pm 0.25$  for the sarcoidosis group. These results suggest a low likelihood that SUR will help

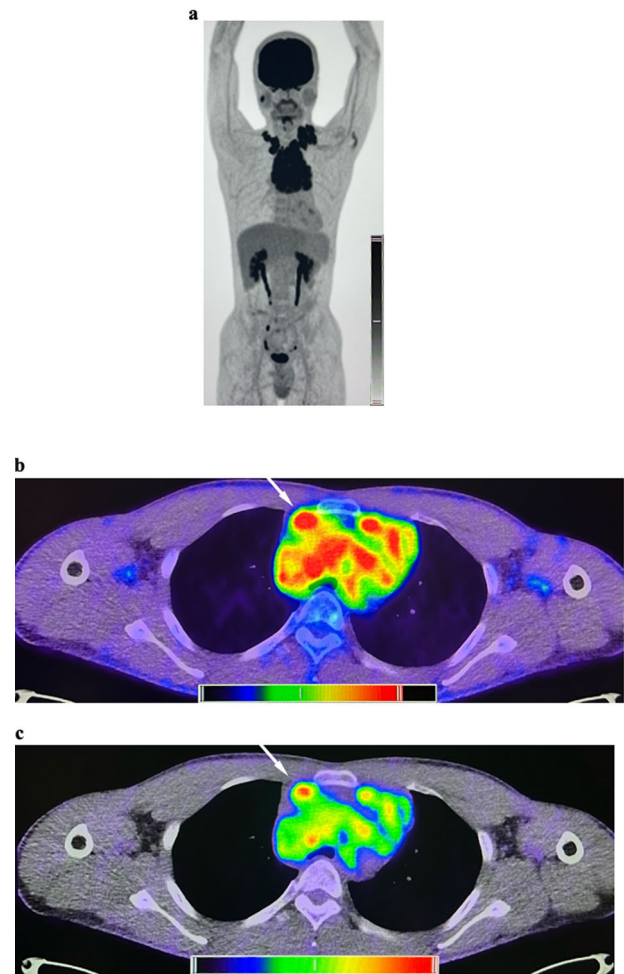


**Fig. 6** A case of a 26-year-old male with Hodgkin lymphoma. MIP image (**a**) demonstrates extensive FDG uptake from the anterior mediastinum to the bilateral supraclavicular fossae. No subdiaphragmatic accumulation is noted. FDG (**b**) and MR<sub>glc</sub> image (**c**) show high FDG uptake in mediastinal lymph nodes (SUV = 6.43, MR<sub>glc</sub> = 3.33). Their values are higher than those of sarcoidosis in Fig. 5. The gray and color calibration scales are shown in the figure. For each scale's window bottom and top values, SUV values were bottom = 0 and top = 5 [SUV-bw], and MR<sub>glc</sub> was bottom = 0 and top = 4 [mg/min/100 mL]. FDG, [<sup>18</sup>F] fluorodeoxyglucose; MIP, maximum intensity projection; MR<sub>glc</sub>, glucose metabolic rate; SUV, standardized uptake value

differentiate malignant lesions from sarcoidosis. Although the fasting time differed between 6 h and 18 h, the difference in blood glucose metabolism was minor. Lymph node activity in sarcoidosis has not been linked to cardiac involvement or response to steroid therapy [15]. It is inferred that the effect of different fasting times on the accumulation of sarcoid lymph nodes is smaller than that on cardiac lesions. Secondly, malignant lesions consist of various pathological types of cancer. Kaneko et al reported that the MR<sub>glc</sub> differed among multiple types of malignant liver tumors [21]. Therefore, limiting the type of carcinoma



as much as possible to distinguish it from benign lesions is useful. Not all cancer patients at our hospital underwent four-dimensional PET/CT protocols. At our hospital, many patients had cancers of the bile duct, liver, and pancreas, resulting in a breakdown of the cancers (Table 2). An ideal study design would be to contrast lymph node metastases from lung cancer with lymph node lesions from sarcoidosis; however, this was not possible because of the small number of patients with lung cancer. Based on this background, malignant lesions included primary and metastatic lesions.

In conclusion, the  $MR_{glc}$  obtained from four-dimensional FDG PET/CT was significantly lower for sarcoid lesions than malignant ones. The use of  $MR_{glc}$  improved sarcoid lesion identification compared with SUV alone. In addition, this implies that four-dimensional FDG PET/CT will lead to the accurate staging of malignant tumors.

#### Abbreviations

AUC	Area under the curve
CS	Cardiac sarcoidosis
DV	Distribution volume
FDG	[ <sup>18</sup> F] Fludeoxyglucose
FDG-6-P	FDG-6-phosphate
GLUT	Glucose transporter
HK	Hexokinase
MIP	Maximum intensity projection
$MR_{glc}$	Glucose metabolic rate
ROC	Receiver operating characteristic
SiPM	Silicon photomultiplier
SUR	Standard uptake ratio
SUV	Standardized uptake value

#### Acknowledgements

We thank all the patients that participated in this study, and the nuclear medicine staff and nursing staff at the Tokyo Women's Medical University Hospital for their commitment to providing excellent care for their patients.

#### Funding

The authors state that this work has not received any funding.

#### Compliance with ethical standards

#### Guarantor

The scientific guarantor of this publication is Michinobu Nagao.

#### Conflict of interest

The authors of this manuscript declare no relationships with any companies whose products or services may be related to the subject matter of the article.

#### Statistics and biometry

No complex statistical methods were necessary for this paper.

#### Informed consent

Written informed consent was obtained from all subjects (patients) in this study.

#### Ethical approval

Institutional Review Board approval was obtained. The study complied with the declaration of Helsinki, and the protocol was approved by the ethics committee of Tokyo Women's Medical University (2021-0153).

#### Study subjects or cohorts overlap

None.

#### Methodology

- Retrospective
- Cross-sectional study
- Performed at one institution

Received: 13 February 2024 Revised: 4 June 2024 Accepted: 5 August 2024

Published online: 16 August 2024

#### References

1. Ungprasert P, Ryu JH, Matteson EL (2019) Clinical manifestations, diagnosis, and treatment of sarcoidosis. *Mayo Clin Proc Innov Qual Outcomes* 3:358–375
2. Cherrett C, Lee W, Bart N, Subbiah R (2023) Management of the arrhythmic manifestations of cardiac sarcoidosis. *Front Cardiovasc Med* 10:1–10
3. Tateishi E, Kiso K (2018) [<sup>18</sup>F]FDG PET/CT for detecting cardiac sarcoidosis. *Ann Nucl Cardiol* 4:151–154
4. Brudin LH, Valind SO, Rhodes CG et al (1994) Fluorine-18 deoxyglucose uptake in sarcoidosis measured with positron emission tomography. *Eur J Nucl Med Mol Imaging* 21:297–305
5. Chang JM, Lee HJ, Goo JM et al (2006) False positive and false negative FDG-PET scans in various thoracic diseases. *Korean J Radiol* 7:57–69
6. Shetty A, Carter JD (2011) Sarcoidosis mimicking lymphoma on FDG-PET imaging. *Radiol Case Rep* 6:409
7. Tamaki N, Hirata K, Kotani T et al (2023) Four-dimensional quantitative analysis using FDG-PET in clinical oncology. *Jpn J Radiol* 41:831–842
8. Rahmim A, Lodge MA, Karakatsanis NA et al (2019) Dynamic whole-body PET imaging: principles, potentials and applications. *Eur J Nucl Med Mol Imaging* 46:501–518
9. Dias AH, Pedersen MF, Danielsen H, Munk OL, Gormsen LC (2021) Clinical feasibility and impact of fully automated multiparametric PET imaging using direct Patlak reconstruction: evaluation of 103 dynamic whole-body [<sup>18</sup>F]FDG PET/CT scans. *Eur J Nucl Med Mol Imaging* 48:837–850
10. Dimitrakopoulou-Strauss A, Pan L, Strauss LG (2012) Quantitative approaches of dynamic FDG-PET and PET/CT studies (dPET/CT) for the evaluation of oncological patients. *Cancer Imaging* 12:283–289
11. Dias AH, Hansen AK, Munk OL, Gormsen LC (2022) Normal values for [<sup>18</sup>F]FDG uptake in organs and tissues measured by dynamic whole-body multiparametric FDG PET in 126 patients. *EJNMMI Res* 12:1–14
12. Fahrni G, Karakatsanis NA, Di Domenicantonio G, Garibotto V, Zaidi H (2019) Does whole-body Patlak [<sup>18</sup>F]FDG PET imaging improve lesion detectability in clinical oncology? *Eur Radiol* 29:4812–4821
13. Chen X, Xu X, Chrysikos S, Zhao M, Zhou Y (2022) Value of 18-fluorodeoxyglucose positron emission tomography/computed tomography ([<sup>18</sup>F]FDG PET/CT) in the differential diagnosis of sarcoidosis and lung cancer with lymph node metastasis: a retrospective study. *Transl Lung Cancer Res* 11:1926–1935
14. Koo HJ, Kim MY, Shin SY et al (2015) Evaluation of mediastinal lymph nodes in sarcoidosis, sarcoid reaction, and malignant lymph nodes using CT and FDG-PET/CT. *Medicine (Baltimore)* 94:e1095
15. Kaneko K, Nagao M, Yamamoto A, Sakai A, Sakai S (2023) FDG uptake patterns in isolated and systemic cardiac sarcoidosis. *J Nucl Cardiol* 30:1065–1074
16. van Sluis J, van Snick JH, Brouwers AH et al (2022) Shortened duration whole body [<sup>18</sup>F]FDG PET patlak imaging on the biograph vision Quadra PET/CT using a population-averaged input function. *EJNMMI Phys* 9:1–14
17. Dias AH, Smith AM, Shah V, Pigg D, Gormsen LC, Munk OL (2022) Clinical validation of a population-based input function for 20-min dynamic whole-body [<sup>18</sup>F]FDG multiparametric PET imaging. *EJNMMI Phys* 9:1–18

18. Dimitrakopoulou-Strauss A, Pan L, Sachpekidis C (2022) Parametric imaging with dynamic PET for oncological applications: protocols, interpretation, current applications and limitations for clinical use. *Semin Nucl Med* 52:312–329
19. Patlak CS, Blasberg RG, Fenstermacher JD (1985) Graphical evaluation of blood-to-brain transfer constants from multiple-time uptake data. Generalizations. *J. Cereb Blood Flow Metab* 5:584–590
20. Naganawa M, Gallezot JD, Shah V et al (2020) Assessment of population-based input functions for Patlak imaging of whole body dynamic [ $^{18}\text{F}$ ]FDG PET. *EJNMMI Phys* 7:67
21. Kaneko K, Nagao M, Yamamoto A et al (2024) Patlak reconstruction using dynamic  $^{18}\text{F}$ -FDG PET imaging for evaluation of malignant liver tumors a comparison of HCC, ICC, and metastatic liver tumors. *Clin Nucl Med* 39:116–123
22. Osborne MT, Hulten EA, Singh A et al (2014) Reduction in [ $^{18}\text{F}$ ] fluorodeoxyglucose uptake on serial cardiac positron emission tomography is associated with improved left ventricular ejection fraction in patients with cardiac sarcoidosis. *J Nucl Cardiol* 21:166–174
23. Gillies RJ, Robey I, Gatenby RA (2008) Causes and consequences of increased glucose metabolism of cancers. *J Nucl Med* 49:24S–42S
24. Jadvar H, Alavi A, Gambhir SS (2009) [ $^{18}\text{F}$ ]FDG uptake in lung, breast, and colon cancers: molecular biology correlates and disease characterization. *J Nucl Med* 50:1820–1827
25. Kaneko K, Sadashima S, Irie K et al (2013) Assessment of FDG retention differences between the FDG-avid benign pulmonary lesion and primary lung cancer using dual-time-point FDG-PET imaging. *Ann Nucl Med* 27:392–399
26. Coelho RG, Calaça IC, Celestrini DM et al (2015) Hexokinase and phosphofructokinase activity and intracellular distribution correlate with aggressiveness and invasiveness of human breast carcinoma. *Oncotarget* 6:29375–29387
27. van den Hoff J, Oehme L, Schramm G et al (2013) The PET-derived tumor-to-blood standard uptake ratio (SUR) is superior to tumor SUV as a surrogate parameter of the metabolic rate of FDG. *EJNMMI Res* 23:77

### Publisher's Note

Springer Nature remains neutral with regard to jurisdictional claims in published maps and institutional affiliations.

Springer Nature or its licensor (e.g. a society or other partner) holds exclusive rights to this article under a publishing agreement with the author(s) or other rightsholder(s); author self-archiving of the accepted manuscript version of this article is solely governed by the terms of such publishing agreement and applicable law.